

PROCEEDINGS OF SPIE

# ***Optics and Photonics for Information Processing VIII***

**Abdul A. S. Awwal  
Khan M. Iffekharuddin  
Mohammad A. Matin  
Andrés Márquez**  
*Editors*

**18–20 August 2014  
San Diego, California, United States**

*Sponsored and Published by*  
SPIE

**Volume 9216**

Proceedings of SPIE 0277-786X, V. 9216

SPIE is an international society advancing an interdisciplinary approach to the science and application of light.

Optics and Photonics for Information Processing VIII, edited by Abdul A. S. Awwal, Khan M. Iffekharuddin, Mohammad A. Matin, Andrés Márquez, Proc. of SPIE Vol. 9216, 921601 © 2014 SPIE  
CCC code: 0277-786X/14/\$18 · doi: 10.1117/12.2087161

Proc. of SPIE Vol. 9216 921601-1

The papers included in this volume were part of the technical conference cited on the cover and title page. Papers were selected and subject to review by the editors and conference program committee. Some conference presentations may not be available for publication. The papers published in these proceedings reflect the work and thoughts of the authors and are published herein as submitted. The publisher is not responsible for the validity of the information or for any outcomes resulting from reliance thereon.

Please use the following format to cite material from this book:

Author(s), "Title of Paper," in *Optics and Photonics for Information Processing VIII*, edited by Abdul A. S. Awwal, Khan M. Iftikharuddin, Mohammad A. Matin, Andrés Márquez, Proceedings of SPIE Vol. 9216 (SPIE, Bellingham, WA, 2014) Article CID Number.

ISSN: 0277-786X

ISBN: 9781628412437

Published by

**SPIE**

P.O. Box 10, Bellingham, Washington 98227-0010 USA

Telephone +1 360 676 3290 (Pacific Time) · Fax +1 360 647 1445

SPIE.org

Copyright © 2014, Society of Photo-Optical Instrumentation Engineers.

Copying of material in this book for internal or personal use, or for the internal or personal use of specific clients, beyond the fair use provisions granted by the U.S. Copyright Law is authorized by SPIE subject to payment of copying fees. The Transactional Reporting Service base fee for this volume is \$18.00 per article (or portion thereof), which should be paid directly to the Copyright Clearance Center (CCC), 222 Rosewood Drive, Danvers, MA 01923. Payment may also be made electronically through CCC Online at [copyright.com](http://copyright.com). Other copying for republication, resale, advertising or promotion, or any form of systematic or multiple reproduction of any material in this book is prohibited except with permission in writing from the publisher. The CCC fee code is 0277-786X/14/\$18.00.

Printed in the United States of America.

Publication of record for individual papers is online in the SPIE Digital Library.



[SPIDigitalLibrary.org](http://SPIDigitalLibrary.org)

---

**Paper Numbering:** Proceedings of SPIE follow an e-First publication model, with papers published first online and then in print and on CD-ROM. Papers are published as they are submitted and meet publication criteria. A unique, consistent, permanent citation identifier (CID) number is assigned to each article at the time of the first publication. Utilization of CIDs allows articles to be fully citable as soon as they are published online, and connects the same identifier to all online, print, and electronic versions of the publication. SPIE uses a six-digit CID article numbering system in which:

- The first four digits correspond to the SPIE volume number.
- The last two digits indicate publication order within the volume using a Base 36 numbering system employing both numerals and letters. These two-number sets start with 00, 01, 02, 03, 04, 05, 06, 07, 08, 09, 0A, 0B ... 0Z, followed by 10-1Z, 20-2Z, etc.

The CID Number appears on each page of the manuscript. The complete citation is used on the first page, and an abbreviated version on subsequent pages. Numbers in the index correspond to the last two digits of the six-digit CID Number.

# Contents

vii	<i>Authors</i>
ix	<i>Conference Committee</i>
xi	<i>Introduction</i>

---

## SESSION 1    LEDS, BIOPHOTONICS, AND MORPHOLOGY

---

9216 02	<b>Impact of LED irradiance on plant photosynthesis and action spectrum of plantlet (Invited Paper) [9216-1]</b>
9216 03	<b>Depth compensation in fluorescence molecular tomography using an adaptive support driven reweighted L1-minimization algorithm [9216-2]</b>
9216 04	<b>Multispectral image restoration of historical documents based on LAAMs and mathematical morphology [9216-3]</b>
9216 05	<b>Oxygen saturation detection aided with the theory of lock-in amplifier [9216-4]</b>
9216 06	<b>Multifunction medical endoscope system with optical fiber temperature sensor [9216-65]</b>

---

## SESSION 2    OPTICAL IMAGING

---

9216 07	<b>A roadmap to global illumination in 3D scenes: solutions for GPU object recognition applications [9216-5]</b>
9216 08	<b>Illumination adaptation with rapid-response color sensors [9216-6]</b>
9216 09	<b>Multiple-samples-method enabling high dynamic range imaging for high frame rate CMOS image sensor by FPGA and co-processor [9216-7]</b>
9216 0A	<b>Optical design and characterization of an advanced computational imaging system [9216-8]</b>

---

## SESSION 3    REAL-TIME SYSTEMS APPLICATION

---

9216 0B	<b>Image analysis algorithms for the advanced radiographic capability (ARC) grating tilt sensor at the National Ignition Facility [9216-9]</b>
9216 0C	<b>Autonomous pedestrian localization technique using CMOS camera sensors [9216-10]</b>
9216 0E	<b>Detecting objects with partial obstruction at the ARC split beam injector images at the National Ignition Facility [9216-12]</b>

# Averaged Stokes polarimetry applied to characterize parallel-aligned liquid crystal on silicon displays

A. Márquez<sup>1,2,\*</sup>, F. J. Martínez<sup>1,2</sup>, S. Gallego<sup>1,2</sup>, M. Ortuño<sup>1,2</sup>, J. Francés<sup>1,2</sup>, A. Beléndez<sup>1,2</sup>, I. Pascual<sup>2,3</sup>

<sup>1</sup>Dept. de Física, Ing. de Sistemas y T. Señal, Univ. de Alicante, Ap. 99, E-03080, Alicante, Spain

<sup>2</sup>I.U. Física Aplicada a las Ciencias y las Tecnologías U. de Alicante, Ap. 99, E-03080, Alicante, Spain

<sup>3</sup>Dept. de Óptica, Farmacología y Anatomía, Univ. de Alicante, Ap. 99, E-03080, Alicante, Spain

## ABSTRACT

Parallel-aligned liquid crystal on silicon (PA-LCoS) displays have become the most attractive spatial light modulator device for a wide range of applications, due to their superior resolution and light efficiency, added to their phase-only capability. Proper characterization of their linear retardance and phase flicker instabilities is a must to obtain an enhanced application of PA-LCoS. We present a novel polarimetric method, based on Stokes polarimetry, we have recently proposed for the measurement of the linear retardance in the presence of phase fluctuations. This can be applied to electrooptic devices behaving as variable linear retarders, and specifically to PA-LCoS. The method is based on an extended Mueller matrix model for the linear retarder containing the time-averaged effects of the instabilities. We show experimental results which validate the predictive capability of the method. The calibrated retardance and phase fluctuation values can then be used to estimate the performance of the PA-LCoS device in spatial light modulation applications. Some results will be given.

**Keywords:** Liquid crystal on silicon displays, parallel aligned, retardance measurement, phase-only modulation, spatial light modulation, flicker, diffractive optics, Stokes polarimetry.

## 1. INTRODUCTION

Parallel aligned liquid crystal on silicon devices (PA-LCoS) have found widespread use as spatial light modulators (SLM) since they allow easy operation as phase-only devices, typically required in many applications. Furthermore they can also be applied as amplitude-mostly devices, thus they are highly versatile devices. LCoS in general, and PA-LCoS in particular, can be used in diffractive optics<sup>[1]</sup>, optical storage<sup>[2]</sup>, optical metrology<sup>[3]</sup>, reconfigurable interconnects<sup>[4][5]</sup>, or quantum optical computing<sup>[6]</sup>, due to their very high spatial resolution and very high light efficiency<sup>[7][8]</sup>.

In the present work it is important to note that from a modeling point of view PA-LCoS displays can be assimilated to linear variable retarders<sup>[7][8]</sup>, then the magnitude of interest to characterize these devices is their linear retardance. Another point to be addressed for a more precise modeling is that LCoS and more specifically PA-LCoS exhibit some flicker or fluctuations<sup>[9]-[14]</sup>, specially digital backplane devices<sup>[15][16]</sup> which are widely used. Then the amplitude of the retardance fluctuation becomes a magnitude of interest for a more accurate characterization and modeling of the device under test. Appropriate techniques to obtain both retardance and flicker values have been demonstrated by our group<sup>[17][18]</sup> and by Ramirez et al.<sup>[19]</sup>, based respectively on simple polarimeter setups, specially the extended linear polarimeter<sup>[18]</sup>. In another recent proposal<sup>[20]</sup>, we demonstrated that a more detailed characterization can be obtained by applying a time-average Stokes polarimetry approach. In combination with a Mueller matrix based model we showed that we can predict the response of the device for every gray level and any kind of state of polarization (SOP) at the system entry. We used this technique in<sup>[21]</sup> to analyse the performance of the digital backplane PA-LCoS for a series of different sequence formats addressed and for various working geometries.

In the present work we want to show additional experimental results which extend the validation of the predictive capability of the method<sup>[20]</sup>. In particular, we present results obtained when applying a digital sequence format showing a larger flicker amplitude, which is interesting to check the validity of the approach in more stringent conditions. This further enables to get a deeper insight into the influence of a series of parameters, such as the sequence format addressed or the input SOP, in PA-LCoS devices when being applied as spatial light modulators.

## 2. GENERAL MODEL AND CALIBRATION

### 2.1 General model

First, let us introduce the model we proposed in<sup>[20]</sup>, based on a time-average Stokes polarimetric technique combined with the Mueller-Stokes formalism<sup>[22]</sup>, which enables to deal both with polarized and with unpolarized light. The approach is not restricted to PA-LCoS devices: it can be in general applied to linear variable retarders whose linear retardance exhibits instabilities. The Mueller matrix  $M_R(\Gamma)$  of a linear retarder with a retardance value  $\Gamma$ , with its fast axis along the X-axis is given by,

$$M_R(\Gamma) = \begin{pmatrix} 1 & 0 & 0 & 0 \\ 0 & 1 & 0 & 0 \\ 0 & 0 & \cos \Gamma & \sin \Gamma \\ 0 & 0 & -\sin \Gamma & \cos \Gamma \end{pmatrix} \quad (1)$$

In<sup>[20]</sup> we showed that a reasonable assumption in the case of PA-LCoS is that temporal evolution of fluctuations  $\Gamma(t)$  can be approximated by a triangular time-dependent profile, which can be characterized by only two parameters: its average retardance  $\bar{\Gamma}$  and its fluctuation amplitude  $a$ , defined as half the maximum-to-minimum value for the fluctuation. Taking into account this time-dependent linear model the averaged matrix for the linear retarder is obtained as:

$$\langle M_R(\bar{\Gamma}, a) \rangle = \begin{pmatrix} 1 & 0 & 0 & 0 \\ 0 & 1 & 0 & 0 \\ 0 & 0 & (\sin a/a) \cos \bar{\Gamma} & (\sin a/a) \sin \bar{\Gamma} \\ 0 & 0 & -(\sin a/a) \sin \bar{\Gamma} & (\sin a/a) \cos \bar{\Gamma} \end{pmatrix} \quad (2)$$

Since PA-LCoS displays are reflective devices, in order to analyze the output SOP, an inversion of the horizontal axis must be considered between the corresponding forward and the backward (right-handed) reference systems, which in the Mueller-Stokes formalism is expressed by the inversion matrix as follows,

$$Inv = \begin{pmatrix} 1 & 0 & 0 & 0 \\ 0 & 1 & 0 & 0 \\ 0 & 0 & -1 & 0 \\ 0 & 0 & 0 & -1 \end{pmatrix} \quad (3)$$

Then, the averaged reflected SOP  $S_{out}$  can be calculated as,

$$\langle S_{out} \rangle = Inv \cdot \langle M_R(\bar{\Gamma}, a) \rangle \cdot S_{in} \quad (4)$$

, where  $S_{in}$  corresponds to the input SOP. Specific input SOPs can be found<sup>[20]</sup> providing simple analytical expressions useful to measure the two parameters in the model,  $\bar{\Gamma}$  and  $a$ . In this sense, if the beam impinging the retarder corresponds to linearly polarized light at  $+45^\circ$  with respect to the X axis, i.e. ( $S_0=1, S_1=0, S_2=1, S_3=0$ ), the average SOP and the degree of polarization, DoP, at the output of the device will be expressed as follows:

$$\langle S_{out} \rangle = \begin{pmatrix} 1 \\ 0 \\ -(\sin a/a) \cos \bar{\Gamma} \\ (\sin a/a) \sin \bar{\Gamma} \end{pmatrix} \quad (5)$$

$$DoP = (\sin a/a) \quad (6)$$

We note that the output  $S_1$  component is zero independently of the retardance and its fluctuation amplitude. The expression for DoP is also straightforward and is directly related to the fluctuation amplitude. Equations (5) and (6) can be used to measure both the average retardance value  $\bar{\Gamma}$  and its fluctuation amplitude  $a$ . This can be easily accomplished using Eq. (6) to obtain the fluctuation amplitude  $a$ , and the ratio between the 3rd and 4th Stokes vector components, i.e.  $-\langle S_3 \rangle / \langle S_2 \rangle = \tan(\bar{\Gamma})$ , to obtain  $\bar{\Gamma}$ .

In the more general case, for an arbitrary input SOP, the resultant average Stokes vector is,

$$\langle S_{out} \rangle = \begin{pmatrix} S_0 \\ S_1 \\ -(\sin a/a)(S_2 \cos \bar{\Gamma} + S_3 \sin \bar{\Gamma}) \\ -(\sin a/a)(-S_2 \sin \bar{\Gamma} + S_3 \cos \bar{\Gamma}) \end{pmatrix} \quad (7)$$

where the Stokes components for the input SOP are  $S_0$ ,  $S_1$ ,  $S_2$  and  $S_3$ , and the corresponding expression for the degree of polarization (DoP) for this average output SOP is given by,

$$DoP = \sqrt{(S_1)^2 + (\sin a/a)^2 ((S_2)^2 + (S_3)^2)} / S_0 \quad (8)$$

We note that the DoP depends on the input SOP and on the amplitude  $a$  of the fluctuations, but it does not depend on the average retardance  $\bar{\Gamma}$ . According to the model proposed<sup>[20]</sup>, Eqs. (2), (7) and (8) provide all the information necessary to calculate the performance of the PA-LCoS device under test and the resulting output light wavefront.

## 2.2 Calibration

We consider a commercial PA-LCoS display, model PLUTO distributed by the company HOLOEYE. It is a nematic liquid crystal filled, with 1920x1080 pixels and 0.7" diagonal, and digitally addressed. By means of a RS-232 interface and its corresponding provided software, we can configure the modulator for different applications and wavelengths. Besides, different pulse width modulation (PWM) addressing schemes (digital addressing sequences) can be generated by the driver electronics<sup>[10][16]</sup>. We have selected two electrical sequences exhibiting a clearly different scale of fluctuations, whose configuration files are provided with the software. They correspond to the configurations labeled as "18-6 633 2pi linear" and "5-5 633 2pi linear".

As already described in<sup>[20]</sup> we obtain the time-averaged polarimetric measurements using a rotating waveplate-based polarimeter, in particular the model PAX5710VIS-T distributed by the company THORLABS. Its software allows different time interval options so as to obtain an averaged signal. When enough rotations are considered, and if the periods of fluctuation and half-rotation are not multiple, then for each angular position of the rotating waveplate the amount of samples collected is representative of the time-varying SOP generated by the fluctuations in the device. The polarimeter averaging time considered is 600 ms, much larger than actually needed to obtain fully stable and repeatable SOP measurements, specially when compared with the time period (frequency) for the fluctuations in our PA-LCoS device is 8.66 ms (120 Hz).

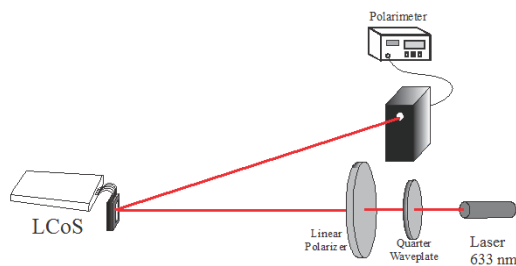


Fig. 1. Experimental setup used to measure linear retardance and flicker with the averaging Stokes polarimetric technique: quasi-perpendicular incidence at 3°.

In Figs. 1 we show the diagram for the characterization setup. The unexpanded beam from a laser (He-Ne laser at 633 nm in this work) incides onto a polarizer with its transmission axis at  $+45^\circ$  with respect to the laboratory vertical (X-axis for the right-handed system used in this work). When using polarized laser light an additional waveplate must be inserted before the polarizer to secure that enough light traverses the polarizer. Light impinges quasi-perpendicularly to the LCoS and the polarimeter head measures the beam reflected from the LCoS. We note that the director axis (extraordinary axis) in nematic based LCoS generally corresponds to the slow axis. In the present LCoS the director axis is along the horizontal.

In Figs. 2(a) and 2(b) we show respectively for the two sequences the average Stokes vector components and the DoP measured with the Stokes polarimeter at quasi-perpendicular incidence at  $3^\circ$ , and for different gray level values addressed onto the LCoS device. Note that in Ref.<sup>[20]</sup> we only analyzed the configuration “5-5 633 2pi linear”, and the results were measured for another typical working geometry: perpendicular incidence with a non-polarizing beam-splitter in front of the LCoS. From the results in Fig. 2(a) we note that parameter  $S_1$  is close to zero in agreement with the expression in Eq. (5). We also see that DoP, Fig. 2(b), is larger for the 5-5 sequence.

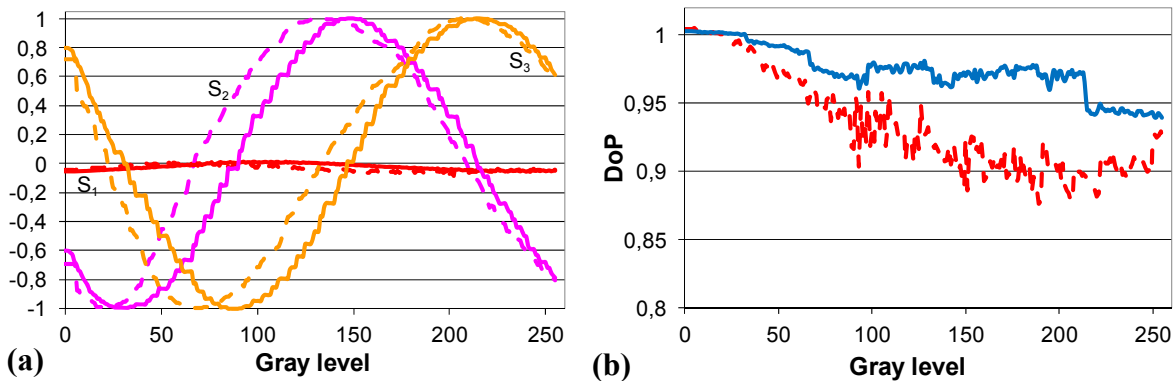


Fig. 2. Experimental values for the: (a) Stokes parameters; (b) the DoP. For input SOP linear at  $+45^\circ$ ,  $\lambda=633\text{nm}$ , and for sequences “18-6 633 2pi linear” (dashed) and “5-5 633 2pi linear” (continuous) at quasi-perpendicular incidence at  $3^\circ$ .

From the results in Fig. 2 and applying Eqs. (5) and (6) according to the characterization approach described in Section 2.1, we can extract the fluctuation amplitude and the average retardance for each gray level. In Fig. 3 we show these results, where we observe that the retardance range is about  $360^\circ$  for both sequences with a very good linearity, specially for the sequence “5-5 633 2pi linear”. The fluctuation amplitude is clearly smaller for the 5-5 sequence with maximum values slightly higher than  $30^\circ$ . The various jumps encountered in the fluctuation amplitude in both sequences reveal the pulsed nature of the digital signal addressed onto the LCoS: more jumps are seen in the 18-6 sequence. For  $\text{DoP} > 1$ , non-physical values, we consider that fluctuation amplitude is  $0^\circ$ .

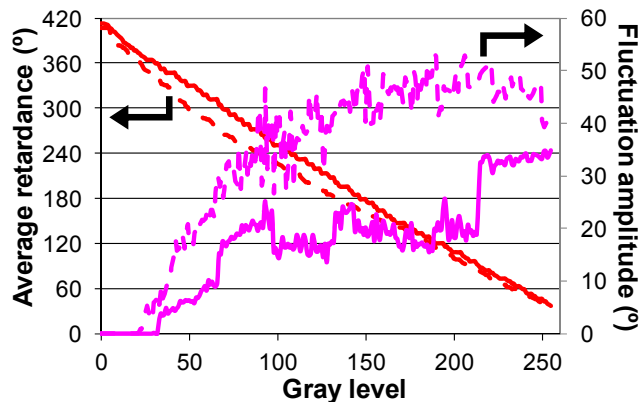


Fig. 3. Calculated values for the average retardance and the fluctuation amplitude for  $\lambda=633\text{nm}$ , and for sequences “18-6 633 2pi linear” (dashed) and “5-5 633 2pi linear” (continuous) at quasi-perpendicular incidence at  $3^\circ$ .

### 3. DIGITAL SEQUENCES AND PREDICTIVE CAPABILITY

Next we introduce in Eqs. (2), (7) and (8) the calibrated retardance and fluctuation values to calculate the reflected Stokes vector for two arbitrary input SOPs, and for the two electrical configurations “5-5 633 2pi linear” and “18-6 633 2pi linear”. In particular we have measured the reflected SOP for an incident light beam linearly polarized at  $15^\circ$  with respect to the lab-vertical, and for right-handed circularly polarized light. These two configurations are quite different from each other in the sense that one of them has the S3 component equal to zero and in the latter case is equal to one, thus they enable to validate the predictive capability of the methodology described in the paper under very different conditions. Furthermore, it can be analyzed the modulation ranges offered by PA-LCoS and how they are affected by fluctuations.

#### 3.1 Configuration “5-5 633 2pi linear”

In this subsection we provide the results obtained for the electrical configuration “5-5 633 2pi linear”. In Fig. 4 and 5 we consider input SOP linear at  $+15^\circ$  with respect to the lab-vertical. First, in Fig. 4(a) and (b) we show respectively the Stokes vector, simulated and measured, on the Poincaré sphere, and the degree of polarization (DoP), simulated and measured, versus the gray level addressed. The representation on the Poincaré sphere is very useful to visualize the dynamic range of output SOPs available for an input SOP as a function of the voltage values (gray levels) addressed. We see that the output SOPs are along a circular trajectory centered on the linearly polarized SOP along the vertical. The dark and gray lines correspond respectively to the simulated and experimental Stokes vectors, which are overlapped with each other, thus showing a very good agreement. This good agreement is also clear in the DoP (Fig. 4(b)), whose value is larger than the one presented in Fig. 2(b) for sequence “5-5 633 2pi linear”. The DoP is the radius of the Stokes vector on the Poincaré sphere representation<sup>[22]</sup>, thus, the trajectory presented in Fig. 4(a) is basically described on the surface of the sphere.

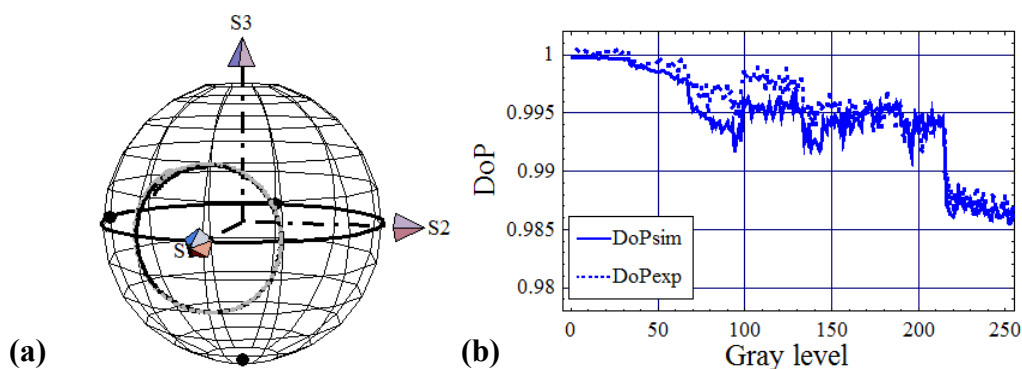


Fig 4. Experiment and simulation, for input SOP linear at  $+15^\circ$ , and  $\lambda=633\text{nm}$ . For sequence “5-5 633 2pi linear”. (a) Plot on the Poincaré sphere of the simulated (dark line) and experimental (grey line) Stokes vectors; (b) Degree of polarization (DoP).

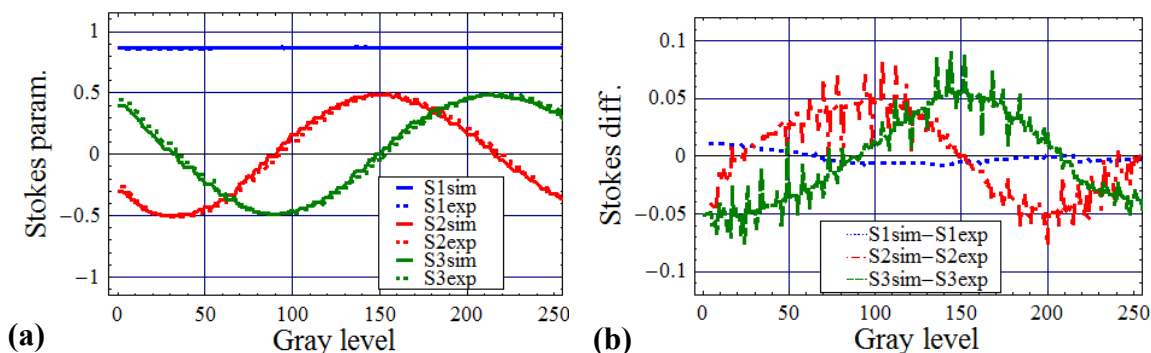


Fig. 5. Experimental and simulated values for the normalized Stokes parameters, for input SOP linear at  $+15^\circ$ , and  $\lambda=633\text{nm}$ . For sequence “5-5 633 2pi linear”. (a) Simulated and experimental values, and (b) their difference.



In Fig. 5 we show an alternative representation of the reflected Stokes vectors results given in Fig. 4(a). We plot in Fig. 5(a) and (b) the normalized Stokes parameters, experimental (dotted lines) and simulated (continuous lines) values and their difference respectively, versus the gray level. Differences between experimental and simulated values are now easier to visualize. First, in Fig. 5(a) we note the constancy of the S1 component and the oscillatory behavior of S2 and S3 components, in accordance with the expression in Eq. (7) where the retardance affects the 3rd and 4th components through the cosine and sine functions. In Fig. 5(b) we see that the profile for the difference between simulation and experiment follows a smooth oscillatory profile smaller than  $\pm 0.05$ , which is a small difference, therefore the model is able to predict the Stokes parameters with a good accuracy across the whole gray level range and the calibration performed enables a full prediction of the average output SOP. Onto the smooth profile we see some sort of noise which we will discuss when we show in Section 3.2 the corresponding results for the configuration “18-6 633 2pi linear”.

Next in Fig. 6 and 7 we show the simulations and measurements for right-handed circularly polarized input SOP. The sort of plots are the equivalent to ones introduced in Fig. 4 and 5. Now we see that the trajectory on the Poincaré sphere is along the meridian lying on the plane S2-S3. We see that both the dark and gray lines (simulation and experiment) are practically overlapped. In Fig. 6(b) the agreement between simulated and measured DoPs is very good, and the corresponding values are larger than in the previous case shown in Fig. 4(b). We may find that the DoP dependence turns to be the same as for the input SOP used for calibration, i.e. Eq. (6). We note that both configurations, linear at  $+45^\circ$  ( $-45^\circ$ ) and circular right-handed (left-handed), are the most sensitive input SOPs, since they provide the largest oscillation amplitude in the measurement of the 3rd and 4th Stokes components, as can be seen in Fig. 6(a), together with the maximum variation of the DoP, shown in Fig. 6(b). In Fig. 7(a) and (b), normalized Stokes parameters, we may appreciate more clearly the agreement between simulation and experiment, in particular in Fig. 7(b), where differences are plotted, with values within  $\pm 0.05$  if the noisy spikes were removed.

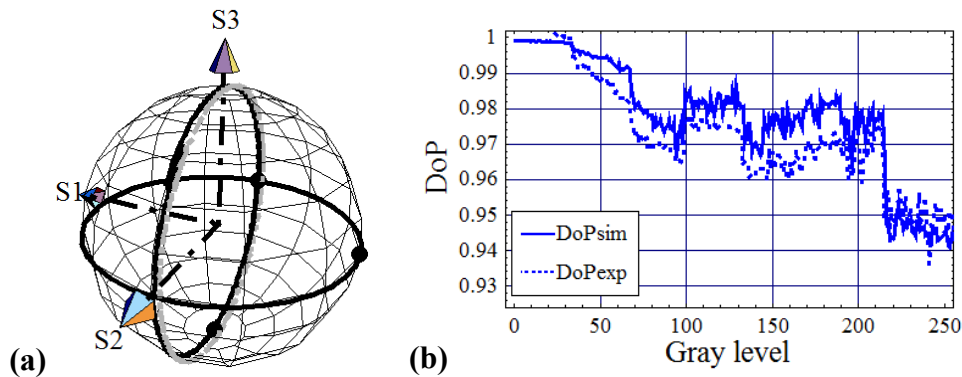


Fig 6. Experiment and simulation, for input SOP right-handed circular, and  $\lambda=633\text{nm}$ . For sequence “5-5 633 2pi linear”. (a) Plot on the Poincaré sphere of the simulated (dark line) and experimental (gray line) Stokes vectors; (b) Degree of polarization (DoP).

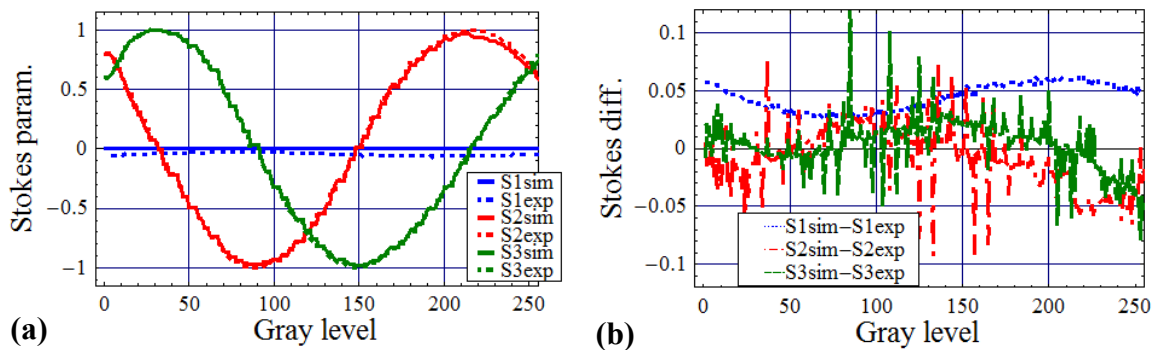


Fig. 7. Experimental and simulated values for the normalized Stokes parameters, for input SOP right-handed circular, and  $\lambda=633\text{nm}$ . For sequence “5-5 633 2pi linear”. (a) Simulated and experimental values, and (b) their difference.

### 3.2 Configuration “18-6 633 2pi linear”

In this subsection we provide the results obtained for the electrical configuration “18-6 633 2pi linear”. In Fig. 8 and 9 we consider input SOP linear at  $+15^\circ$  with respect to the lab-vertical. When compared with the corresponding Fig. 4 and 5, we see that the trajectory on the Poincaré sphere looks very similar, and once again there is a very good agreement between simulation and experiment. This agreement is also very good with the DoP (Fig. 8(b)). Another aspect we appreciate is that the DoP values are now smaller than in Fig. 4(b), which makes sense since fluctuations are larger for the configuration “18-6 633 2pi linear”.

In Fig. 9(b), we see that difference between simulated and measured normalized Stokes parameters is even smaller than it was in Fig. 4(b). It is interesting to note that now there are no noisy spikes as it was the case in Fig. 5(b) and 7(b). It is not fully clear what the reason can be, but it can be related to the smaller amount of quantization levels available with the configuration “5-5 633 2pi linear” (95 levels as described in<sup>[16]</sup>), when compared with “18-6 633 2pi linear” (close to 256 levels), thus the spikes may be indicative of the quantization jumps, therefore discontinuities, in the applied voltage.

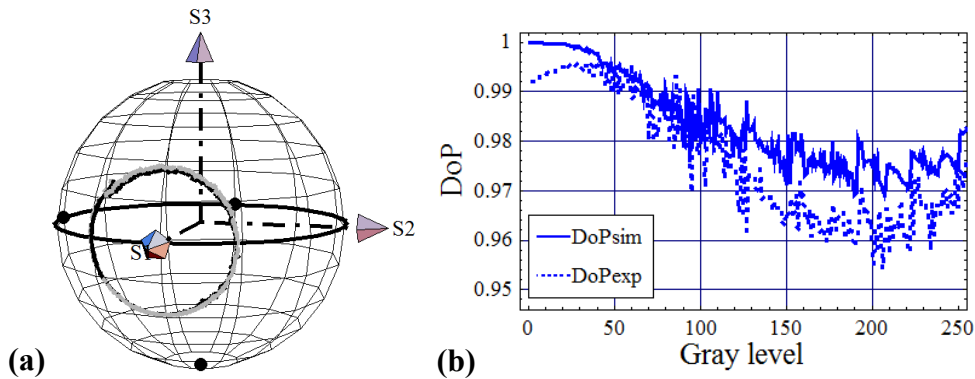


Fig. 8. Experiment and simulation, for input SOP linear at  $+15^\circ$ , and  $\lambda=633\text{nm}$ . For sequence “18-6 633 2pi linear”. (a) Plot on the Poincaré sphere of the simulated (dark line) and experimental (gray line) Stokes vectors; (b) Degree of polarization (DoP).

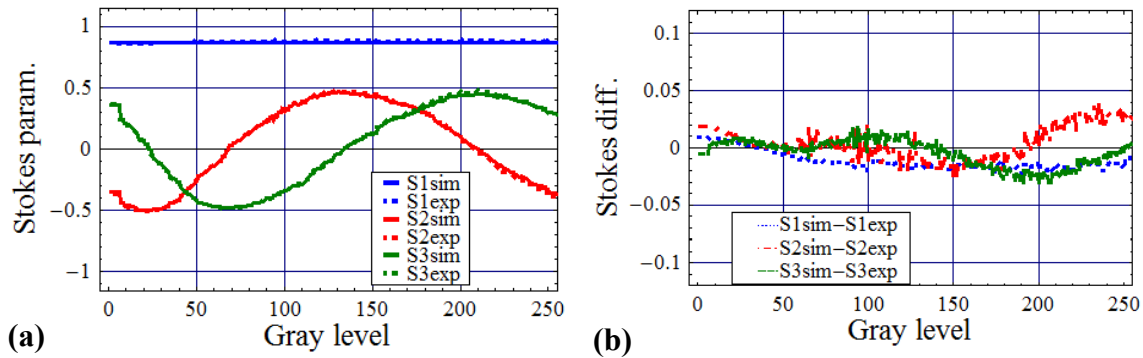


Fig. 9. Experimental and simulated values for the normalized Stokes parameters, for input SOP linear at  $+15^\circ$ , and  $\lambda=633\text{nm}$ . For sequence “18-6 633 2pi linear”. (a) Simulated and experimental values, and (b) their difference.

Next in Fig. 10 and 11 we show the simulations and measurements for right-handed circularly polarized input SOP, which can be compared with the corresponding results in Fig. 6 and 7. In this case we see that DoP (Fig. 10(b)) reaches values smaller than 0.9. Agreement between simulated and measured DoP is almost perfect. Then if we examine differences in the normalized Stokes parameters (Fig. 11(b)) we note that differences are still small, values smaller than  $\pm 0.1$ , but higher than in the previous situations considered for gray levels larger than 100. As in Fig. 9(b) we do not see the deviation spikes which appeared both in Fig. 5(b) and 7(b).

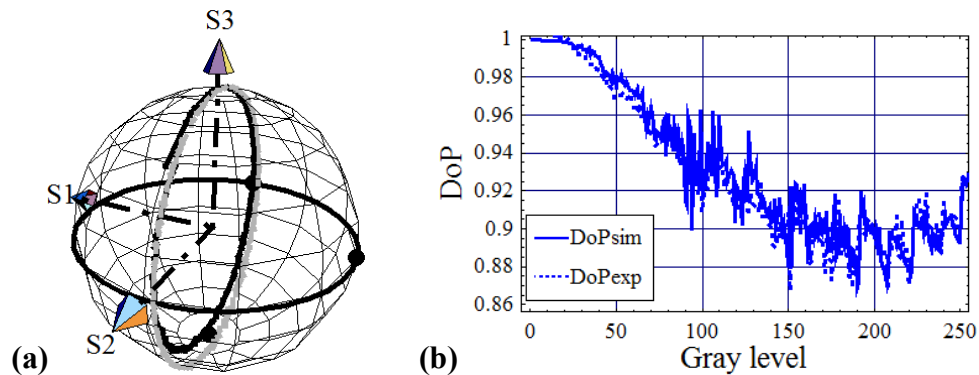


Fig 10. Experiment and simulation, for input SOP right-handed circular, and  $\lambda=633\text{nm}$ . For sequence “18-6 633 2pi linear”. (a) Plot on the Poincaré sphere of the simulated (dark line) and experimental (grey line) Stokes vectors; (b) Degree of polarization.

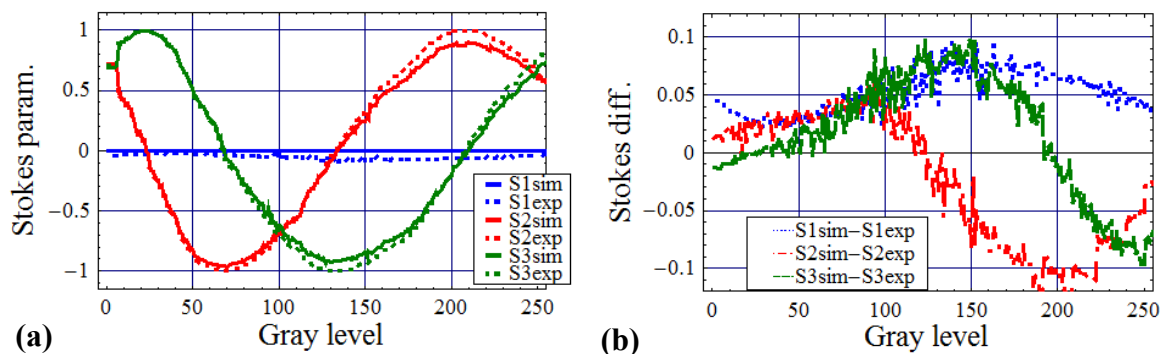


Fig. 11. Experimental and simulated values for the normalized Stokes parameters, for input SOP right-handed circular, and  $\lambda=633\text{nm}$ . For sequence “18-6 633 2pi linear”. (a) Simulated and experimental values, and (b) their difference.

#### 4. CONCLUSIONS

We can conclude that the average Stokes polarimetry technique provides a proper characterization of the linear retardance and its fluctuation magnitude. This has been proved for two electrical configurations showing different magnitudes of fluctuation. The calculation of the Stokes parameters and the DoP has shown very good agreement with the experimental values in all cases, therefore we confirm that both the characterization technique and the Mueller-Stokes model enable to calculate the modulation ranges offered by the PA-LCoS for any arbitrary input SOP considered. From a more general perspective, the characterization provided by the average Stokes polarimetric technique may be useful, on one side, to refine the understanding of the dynamics of liquid crystal devices and, on the other side, to widen their applicability in polarization control, as with experiments dealing with unconventional polarization states<sup>[23]</sup>, where the predictive capability of our Mueller-Stokes model may prove very useful.

#### ACKNOWLEDGEMENTS

This work was supported by the Ministerio de Trabajo y Competitividad of Spain under projects FIS2011-29803-C02-01 and FIS2011-29803-C02-02 and by the Generalitat Valenciana of Spain (projects PROMETEO/2011/021 and ISIC/2012/013).

## REFERENCES

- [1] J. Turunen and F. Wyrowski, eds., [Diffractive Optics for Industrial and Commercial Applications], Akademie Verlag (1997).
- [2] H. J. Coufal, D. Psaltis, and B. T. Sincerbox, eds., [Holographic Data Storage], Springer-Verlag (2000).
- [3] W. Osten, C. Kohler, and J. Liesener, "Evaluation and application of spatial light modulators for optical metrology," *Opt. Pura Apl.* **38**, 71-81 (2005).
- [4] M. A. F. Roelens, S. Frisken, J. A. Bolger, D. Abakoumov, G. Baxter, S. Poole, and B. J. Eggleton, "Dispersion trimming in a reconfigurable wavelength selective switch," *J. Lightw. Technol.* **26**, 73-78 (2008).
- [5] M. Salsi, C. Koebele, D. Sperti, P. Tran, H. Mardoyan, P. Brindel, S. Bigo, A. Boutin, F. Verluise, P. Sillard, M. Bigot-Astruc, L. Provost, and G. Charlet, "Mode-Division Multiplexing of 2 100 Gb/s Channels Using an LCOS-Based Spatial Modulator," *J. Lightw. Technol.* **30**, 618-623 (2012).
- [6] M. A. Solis-Prosser, A. Arias, J. J. M. Varga, L. Rebón, S. Ledesma, C. Iemmi, and L. Neves, "Preparing arbitrary pure states of spatial qudits with a single phase-only spatial light modulator," *Opt. Lett.* **38**, 4762-4765 (2013).
- [7] S. T. Wu and D. K. Yang, [Reflective Liquid Crystal Displays], John Wiley & Sons Inc. (2005).
- [8] N. Collings, T. Davey, J. Christmas, D. Chu, and B. Crossland, "The Applications and Technology of Phase-Only Liquid Crystal on Silicon Devices," *J. Display Technol.* **7**, 112-119 (2011).
- [9] J. E. Wolfe and R. A. Chipman, "Polarimetric characterization of liquid-crystal-on-silicon panels," *Appl. Opt.* **45**, 1688-1703 (2006).
- [10] A. Hermerschmidt, S. Osten, S. Krüger, and Thomas Blümel, "Wave front generation using a phase-only modulating liquid-crystal-based micro-display with HDTV resolution," *Proc. SPIE* **6584**, 65840E (2007).
- [11] J. R. Moore, N. Collings, W. A. Crossland, A. B. Davey, M. Evans, A. M. Jeziorska, M. Komarčević, R. J. Parker, T. D. Wilkinson, and H. Xu, "The silicon backplane design for an LCOS polarization-insensitive phase hologram SLM," *IEEE Photon. Technol. Lett.* **20**, 60-62 (2008).
- [12] A. Lizana, I. Moreno, A. Márquez, C. Iemmi, E. Fernández, J. Campos, and M. J. Yzuel, "Time fluctuations of the phase modulation in a liquid crystal on silicon display: characterization and effects in diffractive optics," *Opt. Express* **16**, 16711-16722 (2008).
- [13] A. Lizana, I. Moreno, A. Márquez, E. Also, C. Iemmi, J. Campos, and M. J. Yzuel, "Influence of the temporal fluctuations phenomena on the ECB LCoS performance," *Proc. SPIE* **7442**, 74420G-1 (2009).
- [14] J. García-Márquez, V. López, A. González-Vega, and E. Noé, "Flicker minimization in an LCoS spatial light Modulator," *Opt. Express* **20**, 8431-8441 (2012).
- [15] G. Lazarev, A. Hermerschmidt, S. Krüger, and S. Osten, "LCOS Spatial Light Modulators: Trends and Applications," in *Optical Imaging and Metrology: Advanced Technologies*, W. Osten and N. Reingand, eds., (John Wiley & Sons, 2012).
- [16] F. J. Martínez, A. Márquez, S. Gallego, M. Ortuño, J. Francés, A. Beléndez, and I. Pascual, "Electrical dependencies of optical modulation capabilities in digitally addressed parallel aligned LCoS devices," *Opt. Eng.* **53**, 067104 (2014).
- [17] A. Márquez, F. J. Martínez, S. Gallego, M. Ortuño, J. Francés, A. Beléndez, and I. Pascual, "Classical polarimetric method revisited to analyse the modulation capabilities of parallel aligned liquid crystal on silicon displays," *Proc. SPIE* **8498**, 84980L (2012).
- [18] F. J. Martínez, A. Márquez, S. Gallego, J. Francés, and I. Pascual, "Extended linear polarimeter to measure retardance and flicker: application to LCoS devices in two working geometries," *Opt. Eng.* **53**, 014105 (2014).
- [19] C. Ramirez, B. Karakus, A. Lizana, and J. Campos, "Polarimetric method for liquid crystal displays characterization in presence of phase fluctuations," *Opt. Express* **21**, 3182-3192 (2013).
- [20] F. J. Martínez, A. Márquez, S. Gallego, J. Francés, I. Pascual, and A. Beléndez, "Retardance and flicker modeling and characterization of electro-optic linear retarders by averaged Stokes polarimetry," *Opt. Lett.* **39**, 1011-1014 (2014).
- [21] F. J. Martínez, A. Márquez, S. Gallego, M. Ortuño, J. Francés, A. Beléndez, and I. Pascual, "Averaged Stokes polarimetry applied to evaluate retardance and flicker in PA-LCoS devices," *Opt. Express* **22**, 15064-15074 (2014).
- [22] G. Goldstein, [Polarized Light], Marcel Dekker (2003).
- [23] T. G. Brown and Q. Zhan, "Focus Issue: Unconventional Polarization States of Light," *Opt. Express* **18**, 10775-10776 (2010).